

Spatially resolved stellar populations in the isolated elliptical NGC 821

Robert N. Proctor¹, Duncan A. Forbes¹, Amy Forestell² & Karl Gebhardt²

¹ Centre for Astrophysics & Supercomputing, Swinburne University, Hawthorn VIC 3122, Australia
 Email: rproctor@astro.swin.edu.au, dforbes@astro.swin.edu.au

² Department of Astronomy, University of Texas at Austin, C1400, Austin, TX 78712
 Email: amydove@astro.as.utexas.edu, gebhardt@astro.as.utexas.edu

5 November 2018

ABSTRACT

We present the analysis of Lick absorption-line indices from three separate long-slit spectroscopic observations of the nearby isolated elliptical galaxy NGC 821. The three data sets present a consistent picture of the stellar population within one effective radius, in which strong gradients are evident in both luminosity-weighted age and metallicity. The central population exhibits a young age of ~ 4 Gyr and a metallicity ~ 3 times solar. At one effective radius the age has risen to ~ 12 Gyr and the metallicity fallen to less than $\sim \frac{1}{3}$ solar. The low metallicity population around one effective radius appears to have an exclusively red horizontal branch, with no significant contribution from the blue horizontal branch evident in some globular clusters of the same age and metallicity. Despite the strong central age gradient, we demonstrate that only a small fraction ($\leq 10\%$) of the galaxy's stellar mass can have been created in recent star formation events. We consider possible star formation histories for NGC 821 and find that the most likely cause of the young central population was a minor merger or tidal interaction that caused NGC 821 to consume its own gas in a centrally concentrated burst of star formation 1 to 4 Gyr ago.

Key words: stars: abundances – galaxies: individual: NGC 821

1 INTRODUCTION

The advent of the Lick system of spectral indices (Worthey 1994) has provided researchers with a useful tool in the disentanglement of age and metallicity effects in the integrated spectra of stellar populations. This tool has already been used to uncover interesting trends in the properties of the stellar populations in the centres of galaxies (e.g. Worthey, Faber & González 1992; Gorgas et al. 1997; Greggio 1997; Trager et al. 2000; Proctor & Sansom 2002; Terlevich & Forbes 2002; Proctor et al. 2004b). However, few studies to date have probed significantly beyond the central regions. Most studies have hence only sampled a small, and perhaps biased, fraction of the galaxy mass. The few studies that probe off-centre regions (e.g. Mehlert et al. 2003; Proctor 2002, Sánchez-Blázquez et al. 2005) generally find metallicity gradients to be strong but both age and $[\text{Mg}/\text{Fe}]$ gradients to be small or non-existent. Here we detail the application of Lick indices to the spatially resolved integrated spectra of NGC 821, which we show to possess strong gradients in both metallicity and age.

NGC 821 is a rare example of an isolated elliptical galaxy. At $m-M = 31.91$ (Tonry et al. 2001) it is the closest early-type galaxy in the isolated galaxy sample of Reda et

al. (2004). Reda et al. showed that NGC 821 conforms to the known scaling relations for elliptical galaxies (i.e. the Fundamental Plane and colour-magnitude relation). It has a moderate luminosity ($M_V = -21.12$) and highly elongated isophotes (E6). An isophotal analysis indicates the presence of an edge-on stellar disk along the major axis (e.g. Goudfrooij et al. 1994; Scorza & Bender 1995; de Souza, Gadotti & dos Anjos 2004). It also reveals disk-like kinematics (Emsellem et al. 2004). Otherwise the galaxy shows no morphological fine structure (Michard & Prugniel 2004; Goudfrooij et al. 1994). In a recent catalogue of galaxy ISM properties, Bettoni, Galletta & Garca-Burillo (2003) measured a dust mass that is at the very low end of the distribution for elliptical galaxies (Forbes 1991), while HI and molecular hydrogen are undetected. The ISM properties of NGC 821 are therefore consistent with stellar mass loss alone and do not require any external origin.

In previous studies, the luminosity-weighted age of the stellar population in the central region of NGC 821 has been measured to be 4.2 Gyr (Denicolo et al. 2005), 7.7 Gyr (Trager et al. 2000), 11.5 Gyr (Caldwell, Rose & Concannon 2003) and 12.5 Gyr (Vazdekis, Trujillo & Yamada 2004).

Thus considerable variation exists in the literature from claims of very young to very old ages.

In this work we use Lick indices to determine the radial profiles in age, metallicity and ‘ α ’-element abundance ratios in NGC 821 out to one effective radius ($1r_e$; the radius within which half the galaxy light is contained). We use the χ^2 -minimisation technique of comparing a large number of indices to SSP models to derive ages and metallicities as outlined in Proctor & Sansom (2002). We find a natural explanation for the range of ages measured in previous studies. We also briefly discuss possible evolutionary histories for NGC 821.

2 DATA

In this paper long-slit spectroscopy of three separate studies of NGC 821 are analysed. Each data set covered a wavelength range suitable for the measurement of Lick indices. Trager et al. (1998) index definitions are used throughout.

The first data set was obtained using GMOS on Gemini (North). These data were collected using a 0.5 arcsec slit positioned along the major axis of the galaxy. The observations covered the wavelength range 4100 – 6930 Å at 3.5 Å resolution and a dispersion of 1.77 Å. Three 30 minute exposures were obtained. The data were reduced using the Gemini pipe-line. Residuals to the wavelength calibration solution were <0.1 Å. The three exposures were co-added prior to the extraction of spectra. During extraction, the spectra were spatially binned to provide a signal-to-noise >20 at all radial positions. Spectra from the central and outer regions are shown in Fig. 1. Reliable index estimates were obtained for 18 Lick indices from Ca4227 to Fe5782. The GMOS observations were obtained as part of the author’s program to measure indices out to large radii ($\sim 2r_e$). Unfortunately, only 1.5 of the 8 hours requested exposure time was actually observed. This constrains the index analysis to within $\sim 1r_e$. Neither Lick-index nor flux-calibration standard stars were observed. The spectra could therefore not be flux calibrated by the normal means, and the indices could not be fully calibrated to the Lick system. The effects of these uncertainties will be discussed in Section 2.1.

The second data set was obtained using the Hobby-Eberly Telescope (HET). These data were originally collected for the purposes of analysis of the spatially resolved stellar kinematics (Forestall & Gebhardt 2005). The data include long-slit spectroscopy along both major and minor axes using a 1 arcsec slit. The observations covered the wavelength range 4300 – 7250 Å at 4.5 Å resolution and a dispersion of 1.95 Å. This wavelength range allowed the accurate measurement of 15 Lick indices from Fe4383 to TiO₁ (NaD was excluded due to the effects of interstellar absorption). The data were reduced and binned as described in Forestall & Gebhardt (2005), but were not flux calibrated. A signal-to-noise suitable for index determination was achieved out to approximately $1r_e$. As with the Gemini data, Lick index standard stars were not observed so the indices could not be fully calibrated to the Lick system (see Section 2.1).

The final data set was obtained from the study of Sánchez-Blázquez et al. (2005; hereafter SB05) as line index measurements. The spectrum from the central region was also supplied for the purposes of calibration of the other

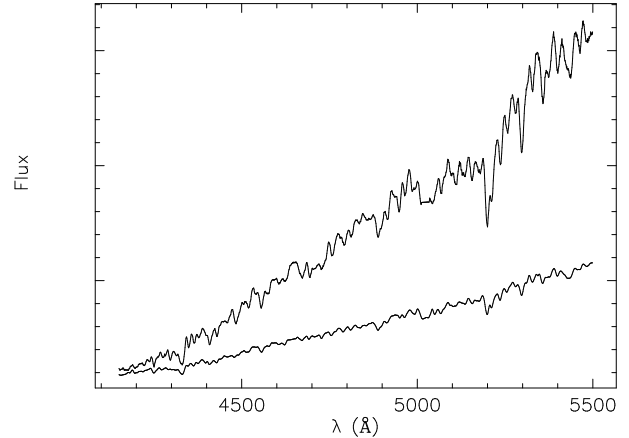


Figure 1. Gemini spectra from the central (upper) and outer (lower) regions of NGC 821 are shown. The spectra have signal-to-noise of 80 and 20 respectively. The presented spectra have been broadened to the Lick resolution of the H β index (8.5 Å) by convolution with a Gaussian. An interpolation across a chip gap is evident at ~ 5000 Å.

two data sets (see Section 2.1). The data were collected using the 3.5 m telescope at the German-Spanish Astronomical Observatory at Calar Alto. Long-slit spectroscopy was carried out with the 2.1 arcsec slit aligned to the parallactic angle, i.e. along a line at 25° to the major axis. The observations covered the wavelength range 3570 – 5770 Å at 2.6 Å resolution and a dispersion of 1.08 Å. This allowed accurate measurement of 19 Lick indices from H δ_A to Fe5335. Although these data were of significantly lower signal-to-noise than the Gemini and HET data, the spectra were accurately flux calibrated prior to index measurements and fully calibrated to the Lick system.

2.1 Calibrations

The calibration of Lick indices is a two stage process. The first is to compensate for the effects of internal velocity dispersion broadening. For the Gemini data velocity dispersions were estimated by cross-correlation of the galaxy spectra with stellar spectra observed with the same instrument configuration. The IRAF command *fxcor* was used. For the HET data set measurements of kinematics were taken from Forestall & Gebhardt (2005). For both Gemini and HET data sets indices were measured and velocity dispersion corrected to the appropriate resolution as described in Proctor & Sansom (2002). For the SB05 data set, both velocity-dispersion corrected indices and kinematics were supplied by the original authors. A comparison of the radially resolved velocity dispersions from the three studies is shown in Fig. 2. Data points are shown at their projected distance from the galaxy centre in this and all other radial plots in this work. Despite the differing slit widths and orientations between the three studies, the comparison in Fig. 2 can be seen to be generally good. Agreement is also good with the central velocity dispersions quoted in the literature (e.g. Bender, Saglia & Gerhard 1994; 208 km s⁻¹, Di Nella et al. 1995; 212 km s⁻¹, Denicolò et al. 2004; 212 km s⁻¹).

The second stage of the calibration to the Lick sys-

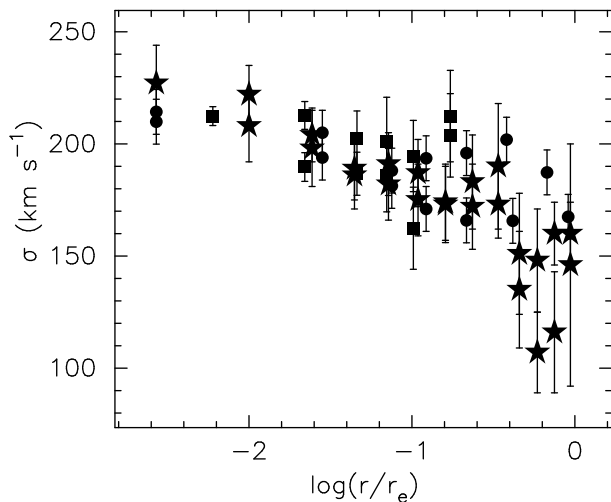


Figure 2. Radial profiles of velocity dispersion from all three data sets. An effective radius of 50 arcsec (de Vaucouleurs et al. 1991) is assumed throughout this work. Gemini data are shown as filled stars, the HET data as filled circles and the SB05 data as filled squares. The agreement between studies is generally good.

tem is to measure offsets between the indices observed in a number of Lick library stars and their published values. This process primarily compensates for differences in flux-calibration between the observations and the stars used to construct the SSP models. The SB05 data set was fully calibrated in this way (using 20 standard stars) and the average offsets supplied with the indices. As noted above, the SB05 spectra were also accurately flux-calibrated. The central spectrum supplied with this data set was therefore used to estimate flux-calibration curves for both Gemini and HET data sets. This was achieved by third-order continuum fitting of the ratio of the fluxed central spectrum from SB05 and the un-fluxed central Gemini and HET spectra. The flux-calibration curves generated were then applied to their respective data sets at all radii. Indices were measured in both flux-calibrated and un-flux-calibrated spectra for the purposes of comparison (see Section 3). We shall refer to these as the fluxed and un-fluxed indices in the Gemini and HET data sets. However, it should be noted the the SB05 spectra did not cover the wavelength range of indices redder than Fe5335. The un-fluxed values of these indices were therefore used throughout this work. Average errors and the index offsets caused by the application of the flux calibration curve are given in Table 1. Both flux and Lick offsets are generally smaller than the average index errors.

Since our analysis probes the low surface brightness outer regions of the galaxy we must consider the effects of scattered light on our index determinations. For the Gemini data this can be achieved by consideration of count rates in regions of the slit that are masked off (there is one region at each end of the slit and two approximately one-third and two-thirds along the length of the slit). Modelling these count rates as scattered light with a Gaussian distribution, it is possible to show that no more than 10% of the light in the most affected regions (the outermost points) can be from scattered light. Such contamination levels would result in the systematic underestimation of the indices by an amount of up to 10% in the outer regions. However, since

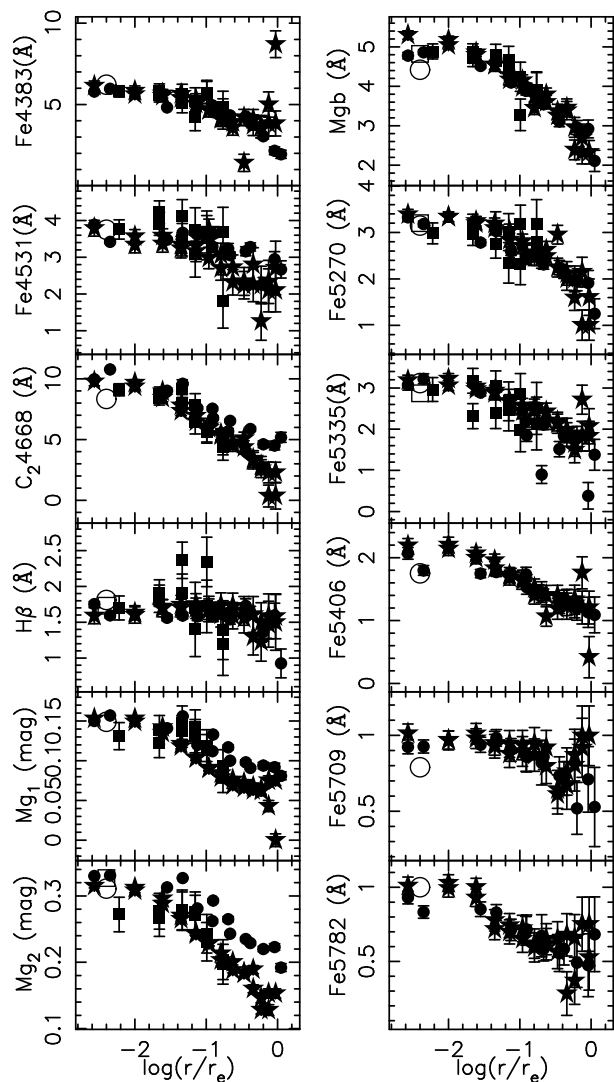


Figure 3. Radial profiles of twelve Lick indices are shown. Filled symbols are as Fig. 2. The central values of Denicolo et al. (2004) (open circles) and González (1993) (open squares) are also shown. Agreement between studies is generally good, with the exception of Mg_1 and Mg_2 (see text). Gradients are evident in all metallicity sensitive indices, while $H\beta$ shows no gradient.

this is an *upper limit* on the contamination levels no attempt has been made to correct indices for this affect. The impact of this uncertainty on our derived ages and metallicities will be discussed in Section 4.

2.2 Radial profiles in indices

Radial profiles of twelve indices (which have been flux-calibrated but not corrected to the Lick system) are shown in Fig. 3. Agreement between the three studies is generally good, despite the differing slit widths and orientations. Mg_1 and Mg_2 are notable exceptions to this good agreement (note the data shown are the values from the flux calibrated spectra). The cause of this discrepancy is not known, but is probably associated with poor flux-calibration of the Gemini and HET data sets. However, this problem does not effect our overall conclusions as the method employed permits the

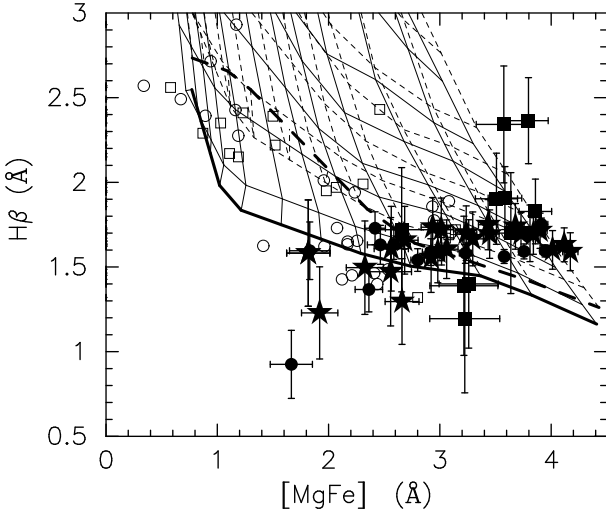


Figure 4. Plot of $H\beta$ against $[MgFe]$. Open circles are the Galactic globular clusters of Proctor, Forbes & Beasley (2004a). Open squares are extra-galactic sub-populations from the meta-study of Strader et al. (2005). Remaining symbols are as Fig. 2. Grid lines show the SSP models of TMB03 (solid lines) and TMK04 (dashed lines) for an ‘ α ’-element enhancement of +0.3 dex. The near horizontal lines show ages; from bottom to top of 15, 12, 10, 8, 5, 3, 2, 1 Gyr. The thick lines denote the oldest age grid lines. The near vertical lines show metallicity; from right to left of +0.4, +0.25, 0.0 -0.25, -0.5, -0.75, -1.0, -1.25, -1.5, -1.75, -2.0 and -2.25 dex. TMB03 models are those for populations with an exclusively red horizontal branch. The poor agreement of the TMK04 SSP models (which include a blue horizontal branch component) with the low metallicity population in NGC 821 is clearly evident. Both sets of models suggest that radial gradients are present in both age and metallicity.

exclusion of such troublesome indices (see Section 3). Negative gradients are evident in all metallicity sensitive indices. The $H\beta$ index, on the other hand, shows no significant gradient.

Instructive index-index plots are shown in Figs 4 and 5*. Fig. 4 shows that in comparison to both Thomas, Maraston & Bender (2003; hereafter TMB03) and Thomas, Maraston & Korn (2004; hereafter TMK04) models, the galaxy appears to possess both age and metallicity gradients. This figure also demonstrates that the central indices in this galaxy exceed those modelled by TMB03 or TMK04. It was therefore necessary to linearly extrapolate the models to an overall metallicity ($[Z/H]$) of +0.8 dex in order to fit these data. It is interesting to note that the low metallicity data points (with $[MgFe] < 2.0$ Å) show much better agreement with the red horizontal branch models of TMB03 (solid lines in Fig. 4) than the models of TMK04 (dashed lines) which include a blue horizontal branch component. Indeed, the galaxy data points appear to follow the locus of those Galactic globular clusters which possess exclusively red horizontal branch morphologies (Proctor et al. 2004a). Fig. 5 also shows the consistency of the data with the SSP models of TMB03 with ‘ α ’-element enhancements of +0.3 dex, indicating that NGC 821 possesses a similar abundance ratio to other bright elliptical

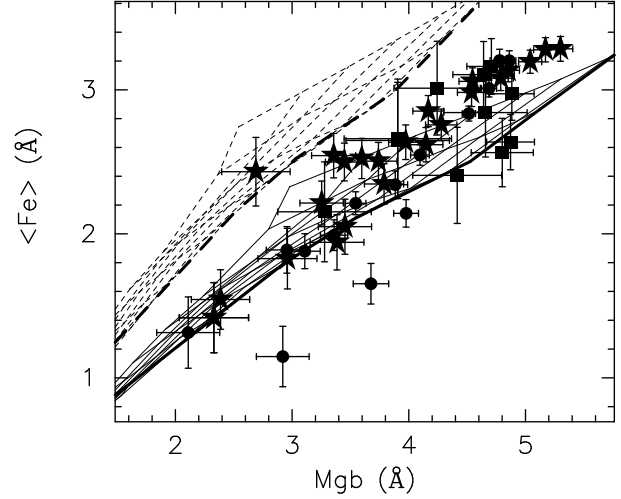


Figure 5. $\langle Fe \rangle$ is plotted against Mgb. Symbols are as Fig. 2. Grid lines show TMB03 models of solar abundance ratio (dashed lines) and ‘ α ’-element enhancement of +0.3 (solid lines). Ages and metallicities of grid lines are as Fig. 4. The data are generally consistent with grid lines with ‘ α ’-element enhancement of +0.3 dex.

galaxies (e.g. Trager et al. 2000; Proctor & Sansom 2002; Mehlert et al. 2003; Proctor et al. 2004b). In the following section we outline the procedure by which values of age and $[Fe/H]$ and the ‘ α ’-element abundance ratio are determined.

3 DETERMINATION OF AGE AND METALLICITY

For all three data sets measurements of $\log(\text{age})$, $[Fe/H]$ and ‘ α ’-abundance ratio (the derived parameters) were made using the χ^2 -minimisation technique detailed in Proctor & Sansom (2002) and Proctor et al. (2004a,b). The ‘ α ’-abundance ratio is parameterised by $[E/Fe]$; the abundance ratio of a group of elements including C, O and Mg (see TMB03 for details). Briefly, the technique for measuring the derived parameters involves the simultaneous comparison of as many observed indices as possible to SSP models. The best fit is found by minimising the deviations between observations and models in terms of the observational errors i.e. χ . The rationale behind this approach is that, while all indices show some degeneracy with respect to $\log(\text{age})$, $[Fe/H]$ and $[E/Fe]$, each index does contain *some* information regarding each parameter. In addition, such an approach should be relatively robust with respect to many problems which are commonly experienced in the analysis of spectral indices. These include poor flux calibration or sky subtraction, stray cosmic rays and central emission (common in LINERs and AGN). The method is also more robust with respect to the uncertainties in the modelling of both the SSPs (e.g. the second parameter effect in horizontal branch morphologies) and abundance ratio effects. It was shown in Proctor et al. (2004a) that, at least for Galactic globular clusters, the results so derived are significantly more reliable than those based on only a few indices.

* $[MgFe] = \sqrt{Mgb \times (Fe5270 + Fe5335)/2}$
 $\langle Fe \rangle = (Fe5270 + Fe5335)/2$

Index	Gemini		HET		SB05	
	Avg error	Flux offset	Avg error	Flux offset	Avg error	Lick Offsets
H δ_A	-	-	-	-	0.687	0.000
H δ_F	-	-	-	-	0.459	0.000
CN $_1$	-	-	-	-	0.018	-0.013
CN $_2$	-	-	-	-	0.021	-0.014
Ca4227	0.204	0.004	-	-	0.304	-0.193
G4300	0.354	0.108	-	-	0.509	-0.346
H γ_A	0.402	0.513	-	-	0.607	0.568
H γ_F	0.251	0.164	-	-	0.371	0.451
Fe4383	0.492	0.082	0.125	-0.059	0.674	0.000
Ca4455	0.254	0.019	0.068	-0.015	0.354	0.201
Fe4531	0.367	0.006	0.110	-0.005	0.507	0.000
C4668	0.531	-0.013	0.190	0.095	0.818	-0.682
H β	0.197	-0.017	0.089	0.032	0.305	-0.104
Fe5015	0.409	-0.029	0.222	0.275	0.665	0.000
Mg $_1$	0.004	-0.003	0.002	0.027	0.019	0.013
Mg $_2$	0.004	-0.004	0.002	0.016	0.028	0.002
Mgb	0.183	-0.001	0.122	-0.010	0.322	-0.157
Fe5270	0.198	0.006	0.143	-0.067	0.365	0.000
Fe5335	0.222	0.001	0.174	-0.047	0.445	0.000
Fe5406	0.166	0.000	0.132	-0.022	-	-
Fe5709	0.121	-	0.113	-	-	-
Fe5782	0.112	-	0.109	-	-	-
TiO $_1$	-	-	0.003	-	-	-

Table 1. Calibration details. For Gemini and HET data sets average errors and the difference in indices caused by the flux-calibration procedure (given as un-fluxed minus fluxed) are shown. Flux offsets are generally smaller than the average errors. For the SB05 data set average errors and the offset to the Lick system derived from observations of standard stars are shown. Lick offsets are of similar magnitude to the average errors.

3.1 Reliability of the method used

In order to further demonstrate the improvement in reliability of derived parameters achieved using the χ^2 -minimisation method over the more traditional use of the H β -[MgFe] index combination, we report a simple, reproducible test. First, we take the index values from a range of SSP models (here we use metallicities from -2.25 to +0.5 dex in 0.25 dex steps and ages of 1, 1.5, 2, 3, 5, 8, 12 and 15 Gyr). Then we perturb each index value of each model SSP to represent the observational error. Here we take the error from a randomly generated Gaussian distribution, the width of which was taken from an actual SB05 observation. A low signal-to-noise observation was selected with Lick index errors close to the maximum we deem suitable for age and metallicity determination (i.e. H β error >0.3 Å). In this way a realistic model data set is generated, whose true ages and metallicities are well defined. Next, we estimate ages and metallicities using the methods to be compared.

The results of such a comparison are shown in Fig. 6. It is clear from Fig. 6 that the χ^2 -fitting of all 25 indices (with an rms scatter about model values of 0.07 dex or 17%) is far superior in accuracy to values derived from the H β -[MgFe] index combination (with an rms scatter about model values of 0.20 dex or 58%). Furthermore, the rms scatter about model values when all the Balmer lines are omitted from the fitting procedure (0.09 dex or 23%) is also much smaller than that achieved using the H β -[MgFe] method.

The rms in metallicity about the model values was 0.1 dex both when all indices were included and when the Balmer lines omitted. For the H β -[MgFe] method this rms

was 0.2 dex. For [E/Fe] rms scatters were ≤ 0.1 dex both when all indices were included and when the Balmer lines were omitted. [E/Fe] can not be estimated using the H β -[MgFe] method.

The improvement in accuracy of our χ^2 -minimisation technique over the traditional H β -[MgFe] method *could* be understood simply in terms of the increased number of both age and metallicity sensitive indices employed. However, we have also demonstrated that excellent results are still obtained *with all the Balmer lines excluded from the derivation*. This emphasises the point above that even metallicity sensitive indices contain *some* information regarding age. This provides one of the main motivations for our use of the χ^2 -minimisation technique.

In the analysis reported above, we have included all 25 Lick indices. Real observations rarely include the full wavelength range, and often other indices must also be omitted (see below). In addition, due to overlapping band definitions, the errors of a number of indices are correlated. We therefore tested more realistic combinations of indices. These were based on the indices used in the analysis of the three data sets below, and included only 15 indices (i.e. excluding H δ_A , H δ_F , CN $_1$, CN $_2$, Ca4455, Mg $_1$, Mg $_2$, NaD TiO $_1$ and TiO $_2$). It should be noted that the excluded indices include the majority of those with correlated errors. The rms scatter when just these 15 indices were included increased to 0.1 dex (26% in derived age), still significantly better than those derived by the H β -[MgFe] method.

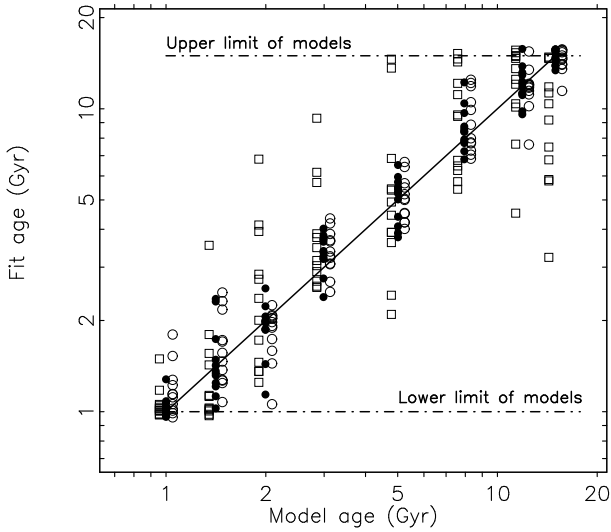


Figure 6. Comparison of ages derived using three different combinations of indices. Filled circles represent results from χ^2 -minimisation of all 25 indices. These results show a scatter of 0.07 dex about the model values. Open circles represent results from χ^2 -minimisation of the remaining 20 indices when the five Balmer lines are excluded. The rms scatter about model values in this case is 0.09 dex. Open squares represent results from the $H\beta$ -[MgFe] technique. These results show an rms of 0.20 dex about model values. The χ^2 -minimisation technique is clearly superior. Indeed, even when all the Balmer lines are excluded from the fitting procedure, the results provide a much improved accuracy over the $H\beta$ -[MgFe] technique.

3.2 Model fitting

In the following analysis we have compared the three sets of observational data to two sets of SSP models; the red horizontal branch (RHB) models of TMB03 and the models of TMK04. As noted previously, Fig. 4 shows that the TMK04 SSP models (which include a blue horizontal branch component) are in poor agreement with the low metallicity population in NGC 821. The models of TMB03, which model purely red horizontal branches, are in much better agreement. Given that other differences between TMB03 and TMK04 models are small the results presented in this work are those derived by comparison to the TMB03 (RHB) models. The comparison to results derived using TMK04 models will be summarised in Section 4.

During the fitting procedure, a number of indices in each data set were found to suffer from problems that make them unsuitable for determining ages and metallicities (see Fig. 7):

- For both Gemini and HET data sets Mg_1 and Mg_2 were found to be aberrant, even in the flux calibrated data (see Fig. 3).
- The Ca4455 index was found to be depressed in all three data sets. This effect has been noted by previous authors in other early-type galaxies (e.g. Worthey 1992; Vazdekis et al. 1997; Trager et al. 1998; Proctor & Sansom 2002).
- In some Gemini/GMOS spectra the Fe5015 index was found to be a poor fit to the models. Subsequent inspection

showed that this occurred when the index fell on a chip-gap interpolation (see Fig. 1).

- Some other individual indices were also found to be poor fits to the data. These were generally associated with sky-line residuals and vignetting (edge) effects in the data.

The indices identified above as giving poor fits to the models were excluded from the fitting procedure. The average deviations of indices to the best fit model values are shown in Fig. 7, where the Mg_1 , Mg_2 and Ca4455 discrepancies are clearly visible.

The effects of flux-calibration and the application of the Lick offsets of SB05 to the Gemini and HET data sets were also investigated. The small offsets in indices caused by flux-calibration (Table 1) had only small effects on the derived parameters. For the Gemini data a difference of $+0.05 \pm 0.05$ dex was found in all three parameters. For the HET data there was an offset in metallicity of $\sim -0.1 \pm 0.05$ dex when flux-calibration was applied. Differences of $+0.05 \pm 0.05$ dex were found in $\log(\text{age})$ and $[E/Fe]$. The χ^2 values of the best fits were found to be marginally lower for the flux-calibrated data. We therefore present data for flux-calibrated spectra in the following.

Differences caused by the application of Lick offsets of SB05 to the Gemini and HET data sets (Table 1) also only caused small offsets in derived parameters ($\log(\text{age})$: -0.08 ± 0.09 , $[Fe/H]$: 0.00 ± 0.07 and $[E/Fe]$: $+0.05 \pm 0.05$). The χ^2 values of the best fits were found to be marginally lower when the Lick offset was *not* applied to the Gemini and HET indices. These offsets were therefore not applied to these data sets in the results that follow.

4 RESULTS

The results of χ^2 -fitting of the data to the RHB models of TMB03 are shown in the left-hand plots of Fig. 8. The Gemini and HET data fitted were those that had been flux-calibrated but without the application of the Lick offsets of SB05. Errors are estimated using 50 Monte Carlo realisations of each data point.

Fig. 8 shows that, generally, agreement between the three studies is good, despite the differing slit widths and orientations. Strong gradients in both age and $[Z/H]$ are evident. Fig. 8 also shows that the age gradient extends from the edge of the seeing affected central region out to $\log(r/r_e) \sim 0.5$, with the population outside this region being uniformly old (i.e. ~ 12 Gyr). The radial $[Z/H]$ gradient (-0.79 dex/dex for points with $-1.7 < \log(r/r_e) < 0.0$) is extremely strong (e.g. Proctor 2002; Mehlert et al. 2003), suggesting that the young, central population formed from highly enriched gas.

Age and metallicity determinations were also made using the Gemini data with all the indices increased by 10%. This was done in order to test the impact of scattered light on the derived parameters in the outer regions of the galaxy (Section 2.1). The resultant ages for the outermost points were identical to those presented here, while $[Fe/H]$ and $[Z/H]$ were increased by 0.1 dex. Given the good agreement between the ages and metallicities from the Gemini data and those from the other two studies (for which we are not able to estimate scattered light directly), we conclude that the

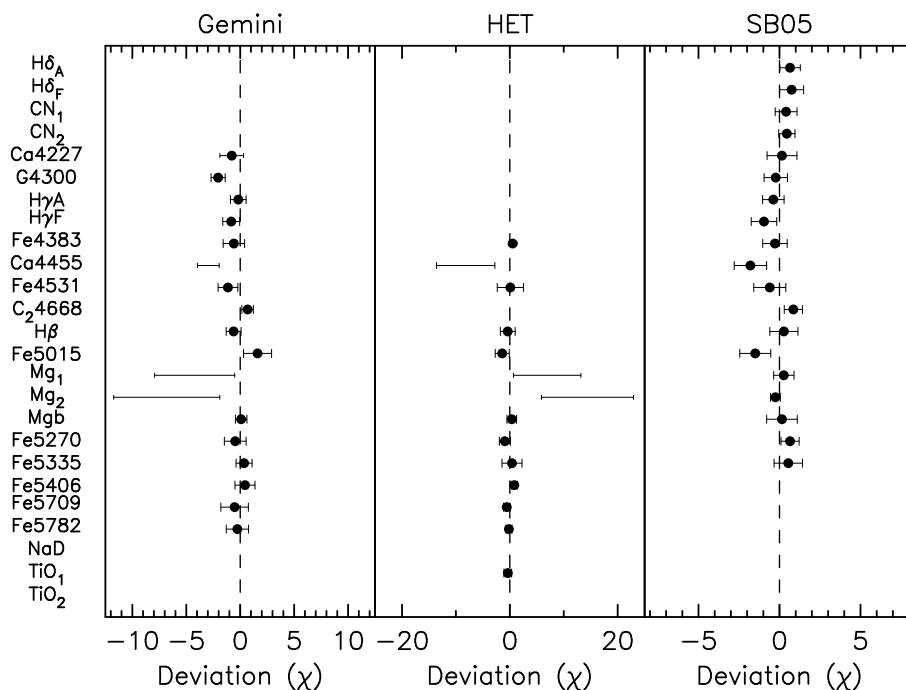


Figure 7. Deviations from best fit values for data compared to the models of TMB03. Mg_1 , Mg_2 and Ca4455 can be seen to be poor fits in the Gemini and HET data. These indices were therefore excluded from the fitting procedure. Ca4455 is also depressed in the SB05 data but its exclusion does not affect the fitting results.

contamination is also $\leq 10\%$ in all three studies. The metallicity gradient given above may therefore be overestimated by as much as 0.1 dex/dex due to scattered light contamination. In addition, the use of TMK04 models results in a slight ($\sim 10\%$) reduction in the metallicity gradient (as well as an increase in central age of ~ 2 Gyr to 6 Gyr). However, even when both scattered light and modelling uncertainties are considered, the metallicity gradient remains steeper than -0.5 dex, leaving the qualitative results outlined below unchanged.

Also indicated in Fig. 8 are estimates of the radii within which 5%, 10%, 20% and 50% of the galaxy’s stellar mass resides. These radii were estimated using the luminosity profile of Ravindranath et al. (2001), an effective radius of 50 arcsec (de Vaucouleurs et al. 1991) and the assumption of a constant stellar mass-to-light ratio. It is evident from Fig. 8 that no more than $\sim 10\%$ of the stellar mass can have been involved in the star formation event responsible for the young central age.

Fig. 8 also shows that the $[E/Fe]$ values in NGC 821 are consistent with no gradient. However, Proctor et al. (2004b) expressed concerns regarding the values of $[Z/H]$ and $[E/Fe]$ that are derived directly from the SSP models. These concerns stem from consideration of the oxygen abundance ratios observed in both the solar neighbourhood, the bulge and the ISM of distant galaxies.

4.1 The local abundance ratio

Oxygen is an important element for two reasons: It is by far the most abundant metal – constituting $\sim 55\%$ of the total metal content of the Sun (Asplund, Grevesse & Sauval 2004). It is a good tracer of Type II supernovae, since its local

Galactic abundance pattern is consistent with it having no other nucleosynthetic sources (Qian & Wasserburg 2001). The oxygen abundance $[O/Fe]$ in the solar immediate neighbourhood (the thin and thick discs and the halo) is approximately $+0.6$ dex at metallicities below $[Fe/H]=-1$. Between $[Fe/H]=-1.0$ and $[Fe/H]=0.0$ $[O/Fe]$ falls from $+0.6$ dex to 0.0 dex (Chiappini, Romano & Matteucci 2003). Bensby, Felzing & Lundström (2003) show that this downward trend in $[O/Fe]$ continues at $[Fe/H]>0.0$, while the abundance ratios of other α -elements (e.g. $[Mg/Fe]$) remain almost constant at the solar value. Fulbright, Rich & McWilliam 2004 have recently shown a similar trend in $[O/Fe]$ with $[Fe/H]$ in Galactic bulge stars, but with $[Mg/Fe]$ elevated with respect to disc stars. The low $[O/Mg]$ ratios implied by these results have also been observed in the ISM of early-type galaxies (Humphrey & Buote 2005 and references therein).

These observations present a challenge to current models of Galaxy formation, and indicate that new physics is required (e.g. see Fulbright et al. 2004). Our concerns are therefore twofold:

- 1) The $[Z/H]$ values assigned to the TMB03 (or any other) SSP models of indices do not include oxygen. Consequently, using the up-to-date solar abundances of Asplund et al. (2004), we calculate that the $[Z/H]$ values at low metallicities are understated by as much as 0.2 dex, while at high metallicities they are overstated by as much as 0.15 dex.

- 2) It is a commonly held belief that *all* $[\alpha/Fe]$ ratios ($[O/Fe]$, $[Ne/Fe]$, $[Mg/Fe]$, $[Si/Fe]$ etc) can act as indicators of formation time-scale in stellar populations. Key assumptions in the reasoning for this belief is that the $[Fe/H]$ of a population is a good proxy for its time of formation (due

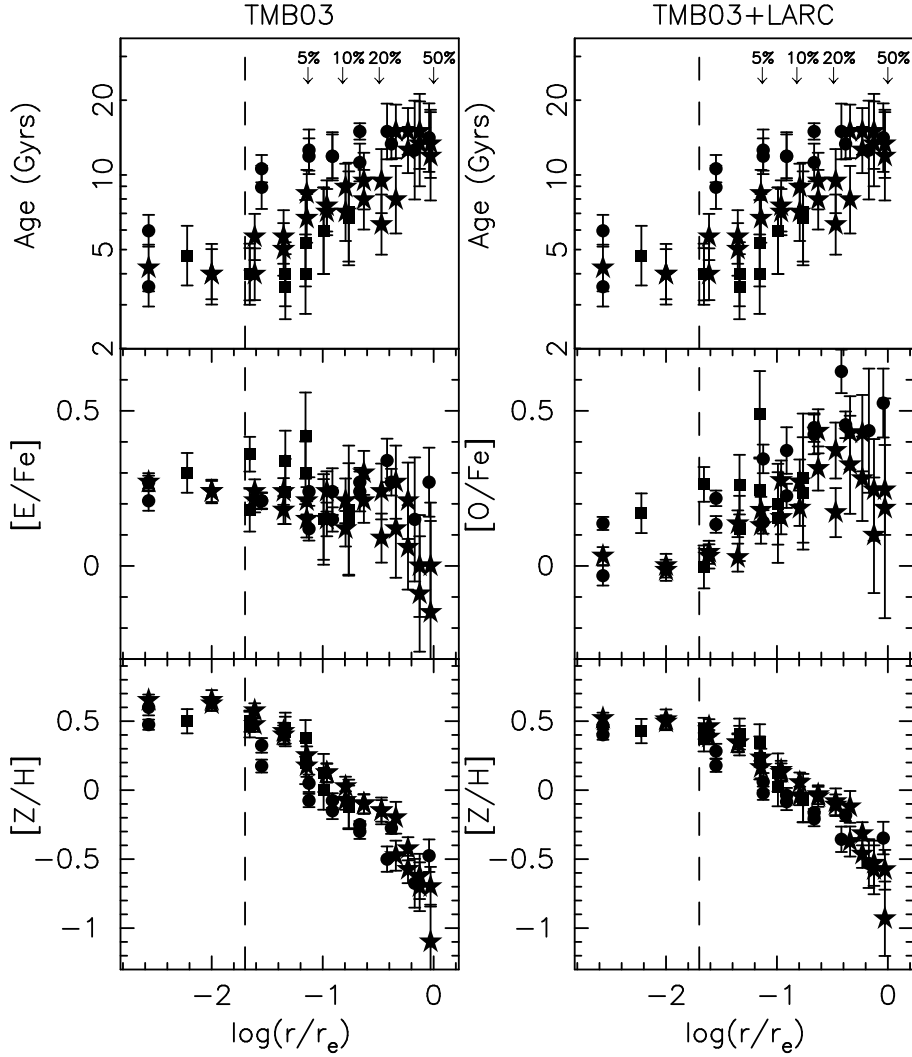


Figure 8. Radial profiles in derived parameters are shown for all three data sets. Symbols are as Fig. 2. The approximate extent of the seeing discs of the three studies are identified by a dashed line. The radii within which 5%, 10%, 20% and 50% of the galaxy’s stellar mass resides are also indicated. Age and metallicity values in the left-hand plots are those derived directly from TMB03 SSP models, while values in the right-hand plots have been LARC corrected (see text). Gradients are evident in both age and $[Z/H]$. However, no gradient is present in $[E/Fe]$ (left-hand plot), while the corrected $[O/Fe]$ (right-hand plot) shows a clear gradient.

to Type Ia supernova production of Fe), while $[\alpha/H]$ is a proxy for the total amount of star formation preceding the formation of the population in question (due to the Type II supernova production of α -elements). The constant $[Mg/Fe]$ and falling $[O/Fe]$ with $[Fe/H]$ in high metallicity disc and bulges stars of our Galaxy clearly indicates a breakdown in one or more of these assumptions. We must therefore either abandon the idea that the $[Fe/H]$ of a population is a proxy for its time of formation (and the belief that $[\alpha/Fe]$ ratios can act as indicators of formation time-scales), or we must accept that not *all* $[\alpha/Fe]$ ratios can act as indicators of formation time-scale in stellar populations.

As a result of these considerations we have applied corrections to the values of $[Z/H]$ to include the effects of the oxygen abundance variations in the stars used to construct the SSP models. Both corrected and uncorrected values are presented in the results that follow.

The correction to $[Z/H]$ was carried out by applying an

offset (ΔZ) to the values derived directly from the TMB03 models using the up-to-date solar abundances of Asplund et al. (2004), the $[O/Fe]$ trend outlined previously. ΔZ was given by:

$$\Delta Z = +0.175 \quad (\text{for } [Fe/H] < -1.0)$$

$$\Delta Z = -0.175[Fe/H] \quad (\text{for } -1.0 \leq [Fe/H] \leq 0.0)$$

$$\Delta Z = -0.33[Fe/H] \quad (\text{for } [Fe/H] > 0.0)$$

Rather than correct $[E/Fe]$ for local trends in $[O/Fe]$, we have chosen to represent the ‘ α ’-element abundance ratio *by* $[O/Fe]$. Both $[E/Fe]$ and $[O/Fe]$ are presented in the results that follow. $[O/Fe]$ was calculated using:

$$[O/Fe] = [E/Fe] + 0.35 \quad (\text{for } [Fe/H] < -1.0)$$

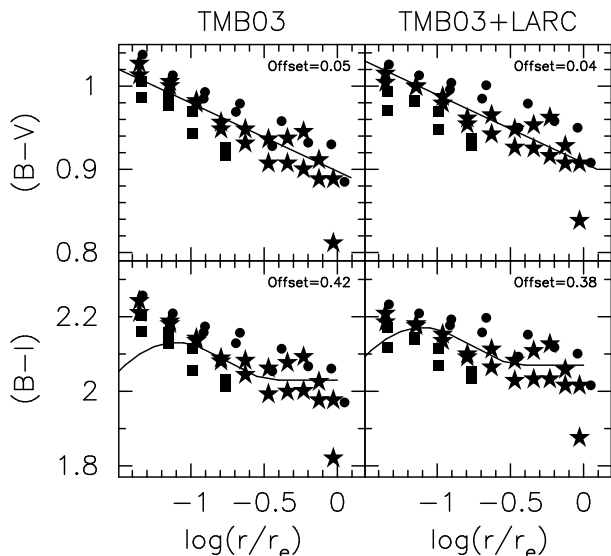


Figure 9. Colours predicted by age and metallicity from TMB03 SSP models and the colours of TMK04. Symbols are as Fig. 2. The radial trends in colours from Goudfrooij et al. (1994) are also shown (lines). However, offsets (given top-right in each plot) have been applied to the Goudfrooij et al. data in order to match our results. These are consistent with the effects of extinction but other contributory factors may be present, such as modelling uncertainties in the SSP models.

$$[\text{O}/\text{Fe}] = [\text{E}/\text{Fe}] - 0.35[\text{Fe}/\text{H}] \quad (\text{for } -1.0 \leq [\text{Fe}/\text{H}] \leq 0.0)$$

$$[\text{O}/\text{Fe}] = [\text{E}/\text{Fe}] - 0.60[\text{Fe}/\text{H}] \quad (\text{for } [\text{Fe}/\text{H}] > 0.0)$$

It is important to note that the expressions given above assume that the $[\text{O}/\text{Fe}]$ with $[\text{Fe}/\text{H}]$ trend in the stellar population under consideration is the same as that in the solar-neighbourhood. This assumption is supported by the fact that in $[\text{O}/\text{Fe}]$ with $[\text{Fe}/\text{H}]$ trends of stars in the bulge of our own Galaxy show an identical trend to the stars in the disc (Bensby et al. 2003; Fulbright et al. 2004), even though the $[\text{Mg}/\text{Fe}]$ of the two populations differ significantly. We shall refer to the correction to $[\text{Z}/\text{H}]$ and the transform from $[\text{E}/\text{Fe}]$ to $[\text{O}/\text{Fe}]$ as the ‘local abundance ratio correction’ (LARC).

There are two significant effects of the local abundance ratio correction on our results for NGC 821. The effect on the $[\text{Z}/\text{H}]$ gradient is to reduce it somewhat (to ~ -0.60 dex/dex), although this is still an extremely strong metallicity gradient. The effect on the slope of the enhancement parameter (now $[\text{O}/\text{Fe}]$) is quite profound, with a gradient evident in $[\text{O}/\text{Fe}]$ that was not present in $[\text{Mg}/\text{Fe}]$. The gradient is such that the young, central population is significantly less enhanced in oxygen with respect to iron than the older, outer regions. This is, at least qualitatively, more in line with expectations, given that we might expect the young, metal-rich population in the centre to have formed from gas that had been enriched by Type Ia supernovae over a longer time-scale than the old population in the outer regions of the galaxy.

As a further test of the derived values of age and metal-

licity, colours were estimated from the models of TMK04 using the age and $[\text{Z}/\text{H}]$ values shown in Fig. 8. Colours for age and $[\text{Z}/\text{H}]$ values derived directly from the TMB03 SSP models are shown in the left-hand plots of Fig. 9, while colours from LARC values are shown in the right-hand plots. These estimates are compared to the photometric observations of Goudfrooij et al. (1994). It was necessary to apply significant offsets (given in the plots) to the Goudfrooij et al. (1994) data in order to obtain a match between our estimates and the observations. The sense of these offsets are consistent with the effects of internal extinction, although other systematic effects (e.g. SSP modelling errors) may be present. However, once this offset is applied the match between observations and data are extremely good, i.e. we recover the relatively shallow colour gradients of Goudfrooij et al. (1994) extremely well, despite the strong age and metallicity gradients present in our spectroscopic results.

5 DISCUSSION

The central luminosity-weighted age of ~ 4 Gyr found in this work is consistent with the young ages found in some previous studies. However, as noted in the introduction, other studies have found *old* ages. We find a natural explanation for these results when we consider the strong age gradient and the varying aperture size between studies. The results presented here for the central regions are for small regions (0.5×0.5 arcsec, 1.0×0.3 arcsec and 2.1×1.1 arcsec for the Gemini, HET and SB05 data sets respectively). Denicolo et al. (2004), who obtain a similarly young age of 4.2 Gyr, used an aperture 1.5×12.0 arcsec, while the Trager et al. (2000) age of 7.7 Gyr was for a 2.0×12.0 arcsec. The two studies that found old ages also used large apertures – Vazdekis et al. (2004) quote an age of 12.5 Gyr within an aperture of 1.6×10 arcsec, while Caldwell et al. (2003) find an age of 11.5 Gyr using a 3×5 arcsec slit. A plot of effective aperture size (using the Jørgensen, Franx & Kjærgaard 1995 definition) the against the measured age shows a correlation, albeit with significant scatter. We therefore conclude that the presence of the age gradient and the varying aperture shapes/sizes between the various studies plays a part in causing the range of ages in the literature.

We next turn our attention to possible star formation histories in NGC 821. The young central age clearly suggests relatively recent star formation, although there is no evidence for *current* star formation. It is therefore appropriate to consider the source of the gas that fuelled this star formation. By making some simple assumptions regarding the relative luminosities of young and old populations we estimate that the mass involved in the more recent burst to be between a few times $\sim 10^8 M_\odot$ (assuming the burst to be 1 Gyr old) and a few times $10^{10} M_\odot$ (assuming the burst to be 4 Gyr old). We therefore constrain the mass involved in the recent starburst to be between $\sim 0.2\%$ and $\sim 10\%$ of the overall galactic mass. These values above are in stark contrast to the current mass of dust ($\sim 2.5 \times 10^5 M_\odot$; Bettoni et al. 2003) and HI gas ($< 10^8 M_\odot$; Georgakakis et al. 2001). It is therefore clear that the gas involved in the recent burst was either almost completely consumed in star formation or

was ejected from the galaxy as a wind.

Next, we consider a number of sources for the gas that fuelled the recent starburst; a major merger, a minor gas-rich merger and in-situ gas.

The first consideration is the extremely strong metallicity gradient present in NGC 821. Such a strong gradient is inconsistent with merger models which predict small gradients due to the ‘washing-out’ of the ambient gradients in the turbulent mixing of the merger (Kobayashi 2004). The gradient in NGC 821 (~ -0.7 dex/dex) is therefore significantly greater than is achieved in merger models. In addition, NGC 821 lacks the tidal tails, shells and plumes expected to persist for ~ 3 Gyr after a major merger (e.g. NGC 1700; Brown et al. 2000). Thus, a recent major merger seems unlikely.

An alternative explanation is that of the accretion of a small, gaseous, satellite galaxy. However, in this scenario, the extremely high central metallicities are hard to achieve since the small accreted galaxy would, presumably, have contained low metallicity gas.

The final scenario we consider is that of a central burst of star-formation fuelled by in-situ gas from the galaxy itself. This could have come from the smooth accretion of cooled halo gas onto a disc as predicted by hierarchical models (e.g. Meza et al. 2003). It is therefore possible that the recent starburst was associated with gas from the embedded stellar disc (Goudfrooij et al. 1994; Scorza & Bender 1995; de Souza et al. 2004). However, Scorza & Bender (1995) show the disc to be highly inclined, with an inclination of $\sim 72^\circ$. Therefore, since the young ages are seen to extend to the same relatively large radii on both major and minor axes (Fig. 8), it is unlikely that the recent starburst was *confined* to the disc.

Regardless of the source of the gas within the galaxy, we would expect the younger population to have ‘ α ’-element abundances depressed with respect to the outer regions. In other words, we would expect the time-scale of star formation to be longer in the young, high-metallicity, central region of NGC 821 than in the old, low-metallicity outer regions. This is clearly not the case for the [E/Fe] values derived directly from TMB03 models. It *is* the case, however, for our estimates of [O/Fe]. We are therefore able to construct a recent star formation history for NGC 821 that is consistent with both spectroscopically determined ages and metallicities and the photometric data by assuming that between 0.2% and 10% of the galaxy’s mass was formed 1 Gyr to 4 Gyr ago, respectively, from the galaxy’s own gas. The paucity of gas remaining within the galaxy favours the lower end of this mass range and younger ages for the recent starburst. This, then, represents our favoured scenario.

6 CONCLUSIONS

We have presented the analysis of Lick indices from three separate long-slit spectroscopic observations of the nearby elliptical galaxy NGC 821. The three data sets have been shown to present a consistent picture of the stellar population within one effective radius. Strong gradients in both age and metallicity were observed. The old ($\gtrsim 10$ Gyr), low metallicity ([Fe/H] ~ -1.0) population in the outer regions

of the galaxy ($r \sim 1r_e$) exhibit no sign of the blue horizontal branch morphologies present in some Galactic globular clusters of the same age and metallicity. We have shown that the large range of ages in the literature is probably the result of the range of aperture sizes and the strong central age gradient.

We therefore find the central region of NGC 821 to have undergone a burst of star formation between 1 Gyr and 4 Gyr ago. This conclusion is based on the 4 Gyr luminosity-weighted age found for the integrated spectra of the central region and the observation that the galaxy, which shows no current star formation, has also passed through the post-starburst phase (which persists for approx. 1 Gyr). The old ages in the outer regions indicate that the burst was centrally concentrated and we have shown that it can not have involved more than 10% of the galaxy’s stellar mass.

We find the most likely scenario to be a very recent (~ 1 Gyr), low mass ($\sim 0.2\%$ of total galaxy mass) starburst in the in-situ gas, perhaps triggered by the accretion of a small (gas poor) satellite galaxy or a tidal interaction. In this scenario, the ambient gas in NGC 821 was consumed in a centrally concentrated burst of star formation. The burst would have had a high [Fe/H], but low [O/Fe], due to the long ($\gtrsim 10$ Gyr) time-scale of star formation in the galaxy.

Acknowledgements

These data were in part based on observations obtained at the Gemini Observatory, which is operated by the Association of Universities for Research in Astronomy Inc., under a cooperative agreement with the NSF on behalf of the Gemini partnership: the National Science Foundation (United States) the Particle Physics and Astronomy Research Council (United Kingdom), the National Research Council (Canada), CONICYT (Chile), the Australian Research Council (Australia), CNPq (Brazil) and CONICET (Argentina). The Gemini program ID is 20041014-GN-2004B-Q-83. The authors acknowledge the data analysis facilities provided by IRAF, which is distributed by the National Optical Astronomy Observatories and operated by AURA, Inc., under cooperative agreement with the National Science Foundation. We thank the Australian Research council for funding that supported this work. K.G. acknowledges NSF CAREER grant AST-0349095. We would like to thank Patricia Sánchez-Blázquez for the provision of data and spectra.

References

- Asplund M., Grevesse N., Sauval J., 2004, Cosmic abundances as records of stellar evolution and nucleosynthesis”, ed. F.N. Bash & T.G Barnes, ASP Conference Proceedings, in press.
- Bender R., Saglia R.P., Gerhard O.E., 1994, MNRAS, 269, 785
- Bensby T., Feltzing S., Lundström I., 2003, A&A, 410, 527
- Bettoni D., Galletta G., Garca-Burillo S., 2003, A&A, 405, 5
- Brown R.J.N., Forbes D.A., Kissler-Patig M., Brodie J.P., 2000, MNRAS, 317, 406
- Caldwell N., Rose J.A., Concannon K.D., 2003, AJ, 125, 2891
- Chiappini C., Romano D., Matteucci F., 2003, MNRAS, 339, 63

- Denicolò et al. 2004, astro-ph/0411100
- Denicolò et al. 2005, astro-ph/0412435
- de Souza R.E., Gadotti D.A., dos Anjos S., 2004, ApJS, 153, 411
- de Vaucouleurs G., de Vaucouleurs A., Corwin H.G., Buta R.J., Paturel G., Fouqué P., 1991, Third Reference Catalogue of Bright Galaxies, Springer-Verlag, New York
- Di Nella H., Garcia A.M., Garnier R., Paturel G., 1995, A&AS, 113, 151
- Emsellem E., Cappellari M., Peletier R.F., McDermid R.M., Bacon R., Bureau M., Copin Y., Davies R.L., Krajnovi D., Kuntschner H., Miller B.W., de Zeeuw, T.P., 1994, MNRAS, 352, 72
- Forbes D.A., 1991, MNRAS, 249, 779
- Forestall A., Gebhardt K., 2005, (in prep)
- Fulbright J.P., Rich R.M., McWilliam A., 2004, Conference proceeding to Nuclei in the Cosmos VIII, Vancouver
- Georgakakis A., Hopkins A.M., Caulton A., Wiklund T., Terlevich A.I., Forbes D.A., 2001, MNRAS, 326, 1431
- González J.J., 1993, Ph.D Thesis, University of California, Santa Cruz
- Gorgas J., Pedraz S., Guzman R., Cardiel N., Gonzalez J.J., 1997, ApJ, 481, 19
- Goudfrooij P., Hansen L., Jorgensen H.E., Norgaard-Nielsen H.U., de Humphrey P.J., Buote D.A., 2005, ApJ, (submitted), astro-ph/0504008.
- Jong T., van den Hoek L.B., 1994, A&AS, 104, 179
- Jørgensen I., Franx M., Kjørgaard P., 1995, MNRAS, 276, 1341
- Greggio L., 1997, MNRAS, 285, 151
- Kobayashi C., 2004, MNRAS, 347, 740
- Mehlert D., Thomas D., Saglia R.P., Bender R., Wegner G., 2003, A&A, 407, 423
- Michard R., Prugniel P., 2004, A&A, 423, 833
- Meza A., Navarro J.F., Steinmetz M., Eke V.R., 2003, ApJ, 590, 619
- Proctor R.N., 2002, Ph.D Thesis, University of Central Lancashire, Preston, UK
(<http://www.star.uclan.ac.uk/~rnp/research.htm>)
- Proctor R.N., Sansom A.E., 2002, MNRAS, 333, 517
- Proctor R.N., Forbes D.A., Beasley M.A., 2004a, MNRAS, 355, 1327
- Proctor R.N., Forbes, D.A., Hau G.K.T., Beasley, M.A., De Silva, G.M., Contreras, R., Terlevich, A.I., 2004b, MNRAS, 349, 1381
- Qian Y.-Z., Wasserburg G.J., 2001, ApJ, 559, 925
- Ravindranath S., Ho L.C., Peng C.Y., Filippenko A.V., Sargent W.L.W., 2001, AJ, 122, 653
- Reda F.M., Forbes D.A., Beasley M.A., O'Sullivan E.J., Goudfrooij P., 2004, MNRAS, 354, 851
- Sánchez-Blázquez P., Gorgas J., Cardiel N., González J.J., 2005, MNRAS, submitted (**SB05**)
- Scorza C., Bender R., 1995, A&A, 293, 20
- Terlevich A.I., Forbes D.A., 2002, MNRAS, 330, 547
- Thomas D., Maraston C., Bender R., 2003, MNRAS, 339, 897 (**TMB03**)
- Thomas D., Maraston C., Korn A., 2004, MNRAS, 351, L19 (**TMK04**)
- Tonry, John L.; Dressler, Alan; Blakeslee, John P.; Ajhar, Edward A.; Fletcher A.B., Luppino G.A., Metzger M.R., Moore C.B., 2001, ApJ, 546, 681
- Trager S.C., Worthey G., Faber S.M., Bustein D., González J.J., 1998, ApJS, 116, 1
- Trager S.C., Worthey G., Faber S.M., González J.J., 2000, AJ 119, 1645
- Vazdekis A., Peletier R.F., Beckman J.E., Casuso E., 1997, ApJS, 111, 203
- Vazdekis A., Trujillo I., Yamada Y., 2004, ApJ, 601, L33
- Worthey G., 1992, Ph.D. Thesis California Univ., Santa Cruz, USA
- Worthey G., 1994, ApJS, 95, 107
- Worthey G., Faber S.M., González J.J., 1992, ApJ, 398, 69